

Growth and magnetic properties of multiferroic $\text{La}_x\text{Bi}_{1-x}\text{MnO}_3$ thin films

M. Gajek,^{1,*} M. Bibes,² F. Wyczisk,³ M. Varela,⁴ J. Fontcuberta,⁵ and A. Barthélemy¹

¹Unité Mixte de Physique CNRS-Thales, Route départementale 128, 91767 Palaiseau, France

²Institut d'Electronique Fondamentale, CNRS, Université Paris-Sud, 91405 Orsay, France

³Thales Research and Technology France, Route départementale 128, 91767 Palaiseau, France

⁴Departament de Física Aplicada i Òptica, Universitat de Barcelona, Diagonal 647, 08028 Barcelona, Spain

⁵ICMAB, CSIC, Campus de la Universitat Autònoma de Barcelona, 08193 Bellaterra, Spain

(Received 20 December 2006; revised manuscript received 17 March 2007; published 11 May 2007)

A comparative study of $\text{La}_x\text{Bi}_{1-x}\text{MnO}_3$ thin films grown on SrTiO_3 substrates is reported. It is shown that these films grow epitaxially in a narrow pressure-temperature range. A detailed structural and compositional characterization of the films is performed within the growth window. The structure and the magnetization of this system are investigated. We find a clear correlation between the magnetization and the unit-cell volume that we ascribe to Bi deficiency and the resultant introduction of a mixed valence on the Mn ions. On these grounds, we show that the reduced magnetization of $\text{La}_x\text{Bi}_{1-x}\text{MnO}_3$ thin films compared to the bulk can be explained quantitatively by a simple model, taking into account the deviation from nominal composition and the Goodenough-Kanamori-Anderson rules of magnetic interactions.

DOI: 10.1103/PhysRevB.75.174417

PACS number(s): 75.60.Ch, 75.47.Lx, 75.47.-m

I. INTRODUCTION

During the past few years, an important interest has raised towards multiferroic materials.¹ Multiferroics are compounds in which several ferroic orders coexist and can be simultaneously ferro- or antiferroelectric as well as ferro- or antiferromagnetic (AF). This multifunctional character may open the way toward other applications in storage media and represent a viable approach to the design of logic architectures.²

Perovskite BiMnO_3 (BMO) is a ferromagnetic (F) insulator^{3,4} for which a ferroelectric character has been claimed.⁵⁻⁷ BMO has a heavily distorted monoclinic structure ($C2$ space group, $a_m=9.54$ Å, $c_m=9.86$ Å, $b_m=5.61$ Å, $\alpha_m=\beta_m=90^\circ$, and $\gamma_m=110.7^\circ$, where m is for monoclinic),⁸ which can also be represented in a pseudotriclinic system ($a_t=c_t=3.93$ Å, $b_t=3.99$ Å, $\alpha_t=\gamma_t=90.4^\circ$, $\beta_t=91.4^\circ$, where t is for triclinic). Interestingly, it is the only manganite showing a ferromagnetic order (Curie temperature $T_C=105$ K, see Refs. 3, 4, and 8) with a single 3+ valence on the Mn site. This behavior is, indeed, unprecedented as all nondoped manganites are antiferromagnetic. For instance, the LaMnO_3 system displays an A -type antiferromagnetic order⁹ despite the fact that La is isovalent to Bi and has roughly the same ionic radius.¹⁰ In LaMnO_3 , the degeneracy of the Mn e_g levels is lifted by a static Jahn-Teller effect, which causes a cooperative orbital ordering in the (b,c) plane of the perovskite structure.

While an equivalent mechanism occurs in BMO, Bi $6s^2$ lone pairs¹¹ play also a crucial role because of their high stereochemical activity triggering a specific three-dimensional (3D) orbital ordering of the Mn $d_{x^2-z^2}$ orbitals.¹² As a result, ferromagnetic superexchange paths between neighboring Mn are favored over the antiferromagnetic ones. This exotic orbital ordering has been recently characterized by precise structural refinements using neutron diffraction on bulk samples¹² and by resonant x-ray scattering on thin films.¹³

BMO is a highly metastable compound in bulk form and its fabrication requires extreme conditions.⁴ Nevertheless,

BMO can be grown in thin-film form by means of epitaxial stabilization techniques with a pseudomorphic growth.¹⁴ An additional approach in the stabilization of this compound is a slight La substitution (10%). Few groups have studied the physics of solid solutions of LaMnO_3 and BiMnO_3 perovskites.^{15,16} According to Troyanchuk *et al.*,¹⁵ the phase diagram of $\text{La}_x\text{Bi}_{1-x}\text{MnO}_3$ shows two main regions. For $x>0.35$, the compounds are weak ferromagnets. For larger Bi concentrations, these authors state that the system is most likely a mixture of ferromagnetic and antiferromagnetic regions. The spontaneous magnetization grows sharply on going from $x=0.2$ to $x=0.1$, and shows a structural phase transition from orthorhombic to monoclinic. Bulk $\text{La}_{0.1}\text{Bi}_{0.9}\text{MnO}_3$ (LBMO) has a T_C of about 95 K (Ref. 15) and is, therefore, structurally and magnetically very similar to BiMnO_3 .

A few groups have reported on the growth and magnetic properties of BMO in thin-film form.^{6,17-21} Particularly puzzling is the recurrent observation of a reduced magnetization in BMO films compared to bulk, which has been tentatively ascribed to strain effects.^{18,20} Yet, none of these studies have addressed the issue of the reduced magnetization of the samples after a detailed structural and compositional characterization.

In this article, we report on the epitaxial growth of LBMO films on (001) SrTiO_3 (STO) in a narrow range of temperatures (600–650 °C) and pressures (5×10^{-2} – 4×10^{-1} mbar). In agreement with previous reports on BMO films,^{17,18,20,21} magnetization measurements reveal that the films have a fairly reduced moment with respect to the bulk value. We find that this moment is clearly related to changes in the unit-cell volume rather than to strain effects. The variation of the unit-cell volume likely reflects the presence of Bi vacancies as this species is strongly volatile. We, thus, propose a simple scenario explaining the decrease of the magnetization by the presence of Bi vacancies that disrupt the 3D orbital order and modify the Mn valence. A quantitative agreement with the data is obtained and this picture is

supported by x-ray magnetic circular dichroism (XMCD) measurements.

II. EXPERIMENT

The films used in this study have been grown by pulsed laser deposition using a KrF laser ($\lambda=248$ nm) at a frequency of 2 Hz and with a fluence ranging from 1.3 to 2.2 J/cm² (Ref. 22). The target was a pressed pellet from a stoichiometric mixture of La, Bi, and Mn (relative La:Bi:Mn ratio: 1:9:10) oxides positioned at 5 cm of the substrate and rotating at 0.8 Hz during growth. (001)-oriented STO single crystals were used as substrates. They were glued on the substrate holder by silver paste and brought to growth temperature T_S with a resistive heater. The temperature was measured during the whole process with a platinum-rhodium thermocouple embedded in the substrate holder. The growth pressure P_{O_2} was varied from 0.01 to 0.4 mbar of pure oxygen.

STO is a cubic perovskite with a unit-cell parameter of 3.905 Å. Since no structural study has been published on bulk LBMO, the precise mismatch between LBMO and STO cannot be calculated, but it is expected to be close to that with BiMnO₃ (−0.63% for a_t and c_t , −2.1% for b_t). X-ray diffraction (XRD) experiments have been carried out with a Philips MRD system, with the Cu $K\alpha$ radiation. Magnetic measurements have been performed with a Quantum Design superconducting quantum device interferometer, at temperatures ranging from 10 to 350 K, and with fields up to 55 kOe applied in the plane. Emery paper was used to remove the silver paste from the back of the substrate prior to the magnetization measurements. The diamagnetic signal due to the substrate was corrected by measuring the high-field susceptibility of the sample at 150 K, beyond the T_C of LBMO. Chemical characterizations were realized by Auger spectroscopy using an ESCALAB system on the Bi-QV, Mn-LMM transitions. X-ray absorption spectroscopy (XAS) and XMCD measurements were carried out at the SU23 line of the Laboratoire pour l'Utilisation du Rayonnement Electromagnétique (LURE), Orsay, France.

III. RESULTS

A. Phase diagram

Figure 1(a) shows 2θ - ω XRD patterns of 30 nm LBMO thin films grown between $T_S=575$ and 675 °C. At 575 °C, the diffraction curve displays numerous peaks characteristic of the presence of Bi-rich phases, namely, α -Bi₂O₃ and β -Bi₂O₃. In contrast with low-temperature growth, diffraction patterns of films deposited at 675 °C reveal peaks at 38.0° and 81.8°, corresponding to the (004) family of reflections of the haussmanite (Mn₃O₄) phase. No spurious phases are visible on XRD patterns for films grown at 625 and 650 °C. For these temperatures, the diffraction patterns yield only LBMO (0 k 0)_t reflections which shows that the films grow epitaxially with the b_t axis out of plane. Such a growth orientation is preferential because the mismatch of the STO substrate with the b_t axis of LBMO is larger than with the corresponding a_t and c_t axes. It is worth to mention that the

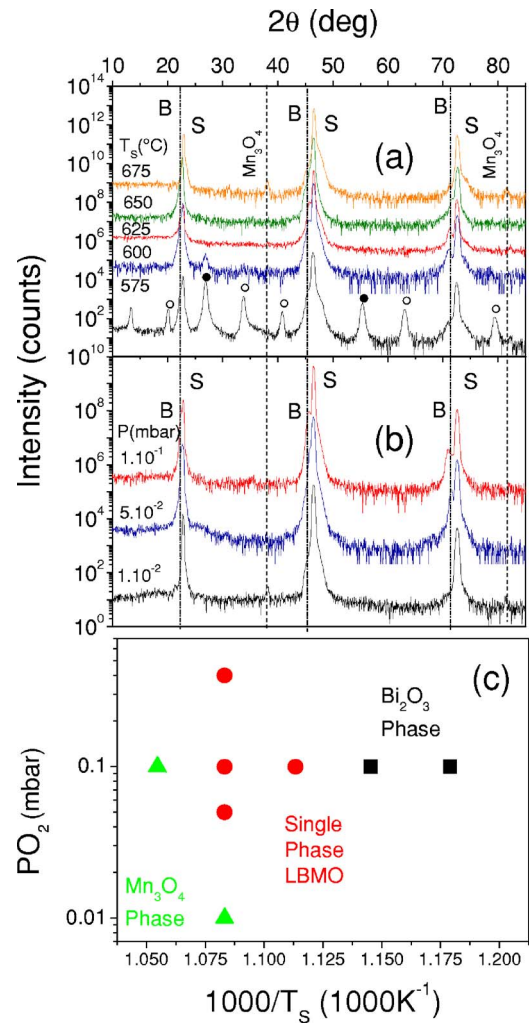


FIG. 1. (Color online) (a) XRD spectra for five films grown at 1.10^{-1} mbar and different temperatures. (b) Spectra for three films grown at 625 °C and different pressures. The peaks are indexed as B, LBMO; S, STO; •, β -Bi₂O₃; ○, α -Bi₂O₃. Vertical dotted-dashed and dashed lines correspond to the position of the diffraction peaks of LBMO and Mn₃O₄, respectively. (c) Pressure-temperature phase diagram for LBMO thin films with a nominal thickness of 30 nm.

texture of the films is the same as that of the substrates, as shown on the ϕ scans of the Fig. 3(d). In these scans, no doubling of the (130)_t LBMO peaks from an eventual twinning could be resolved, which suggests that the LBMO has a tetragonal unit cell in these films.

Diffraction patterns of films grown at a fixed substrate temperature $T_S=625$ °C and different oxygen pressures P_{O_2} are shown on Fig. 1(b). Films grown at 10^{-2} mbar display the characteristic peaks of the Mn₃O₄ phase. For films deposited at higher pressures ($P_{O_2} \geq 5 \cdot 10^{-2}$ mbar), only the LBMO (0 k 0)_t reflections are detected.

These characterizations are summarized in the phase diagram of Fig. 1(c). The temperature range for good quality film deposition is rather narrow (less than 50 °C). This is likely to result from the high volatility of Bi which is an issue for numerous Bi-based compounds, largely reported in the literature.^{23–25} Thus, the apparition of Mn₃O₄ at high

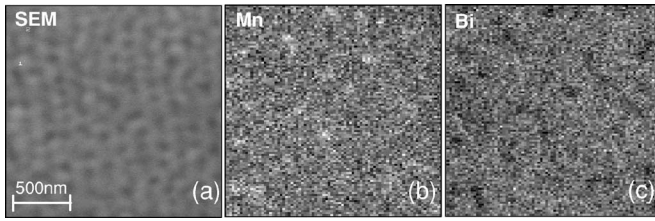


FIG. 2. SEM image (a) and corresponding AES mappings for Mn (b) and Bi (c).

temperatures is probably the result of the formation of Bi vacancies in the perovskite structure. Interestingly, such clusters of Mn-rich spurious phases have already been found to occur in the $\text{La}_{1-x}\text{MnO}_3$ system for $x > 1/8$ (Ref. 26) and ascribed to the collapse of the perovskite structure. We note that a very recent paper has also reported the presence of Mn_3O_4 inclusions in BMO films grown at low pressure,²¹ in agreement with our results.

On the opposite part of the phase diagram, i.e., at low T_S and/or high P_{O_2} , Bi oxides form. The same occurs in films deposited at optimal T_S and P_{O_2} but higher laser frequencies (10 Hz, not shown). The formation of Bi oxides is thus probably the result of insufficient mobility at the surface of the sample. We note that our growth conditions are different from those reported by Eerenstein *et al.*²⁷ for pure BMO films ($T_S=450$ °C and $P_{\text{O}_2}=1.10^{-6}$ mbar). However, the latter are not inconsistent with the phase diagram of Fig. 1(c), since low pressure allows to maintain a high energy of the species on the surface of the substrate at low deposition temperatures and thus limit both Bi evaporation and the formation of Bi oxides.

B. Compositional analysis

Scanning electron microscopy (SEM) with Auger electron spectroscopy (AES) analysis was used to map the chemical composition of samples grown at 625 °C and 1.10^{-1} mbar, i.e., in the middle of the growth window. Composition mappings of Mn and Bi are, respectively, represented on Figs. 2(b) and 2(c). A SEM micrograph of the corresponding area is also shown on Fig. 2(a). These characterizations reveal inhomogeneities of Mn concentrations with the notable presence of 50–100 nm wide Mn-rich clusters. These areas coincide effectively with Bi deficient areas of Fig. 2(b). Such clusters are thus likely to be composed of a Mn oxide, undetected by XRD. A numerical treatment of the contrast of the image of Fig. 2(c) reveals that the quantity of clusters with respect to the rest of the film amounts to about 12%.

C. Structural determinations

In order to obtain more precise structural information on the LBMO phase, additional XRD measurements were performed. An enlargement of the $(020)_i$ reflection of the LBMO close to the STO (002) peak is shown in Fig. 3(a) for films grown at 1.10^{-1} mbar and different temperatures. The $(020)_i$ LBMO peak is shifted from 45.61° to 45.91° when the deposition temperature varies from 600 to 650 °C. This cor-

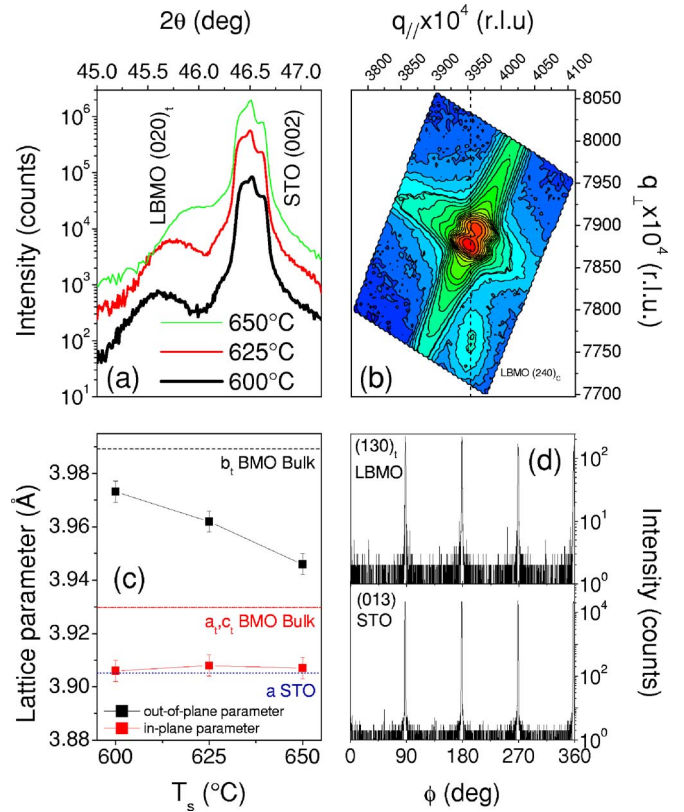


FIG. 3. (Color online) (a) 2θ - ω symmetric XRD scans close to the $(020)_i$ reflection of LBMO and (002) reflection of STO for three 30 nm films grown at 1.10^{-1} mbar and different temperatures. (b) Reciprocal space map close to the $(240)_i$ reflection of LBMO and (204) reflection of STO for a film grown at 625 °C. r.l.u. is for reciprocal lattice units. (c) Evolution of the LBMO unit-cell parameters with the growth temperature. (d) ϕ scan of the (013) reflection of the STO substrate (bottom panel) and the $(130)_i$ LBMO reflection (top panel) for a film grown at 625 °C.

responds to a decrease of the LBMO out-of-plane parameter from 3.97 to 3.94 Å. To check if this variation is accompanied by a change in the in-plane parameter, reciprocal space maps (RSMs) were collected. A RSM close to the $(240)_i$ reflection of a film grown at 625 °C is shown on Fig. 3(b). The LBMO $(240)_i$ reflection appears at the same value of the in-plane reciprocal lattice parameter as for the (204) reflection of the STO substrate, which indicates that the film is in a fully strained state. By performing the same analysis for films grown at 600 and 650 °C, the variation of both the out-of-plane and in-plane parameters as a function of the growth temperature has been determined. As can be seen in Fig. 3(c), the decrease of the out-of-plane parameter with the deposition temperature is uncorrelated with the value of the in-plane parameter which stays constant at 3.905 Å within the experimental error. This reflects a decrease of the unit-cell volume as T_S increases.

The observed decrease of the LBMO unit-cell volume with deposition temperature is probably due to a change in the film composition. A variation of the oxygen concentration is possible but is not the main factor as the presence of oxygen vacancies is known to increase the cell volume in the

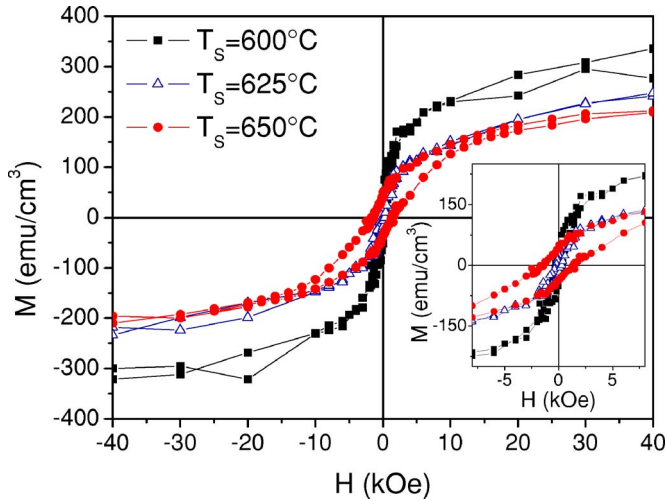


FIG. 4. (Color online) Ferromagnetic hysteresis loops at $T=10$ K of 30 nm LBMO films grown at 1.10^{-1} mbar and different growth temperatures. Inset: zoom of the low-field regime.

perovskite phase [as shown for the LaMnO_3 system²⁸ as well as for ferroelectric perovskites, such as BaTiO_3 (Ref. 29) and PbTiO_3 (Ref. 30)]. On the other hand, a cationic deficiency on the A site of the perovskite structure could explain the diminution of the cell volume, as reported for $\text{La}_{1-\delta}\square_{\delta}\text{MnO}_3$ (where δ is the concentration of vacancies at the A site labeled as \square).³¹ Considering the high volatility of the Bi species, it is reasonable to assume that Bi vacancies are present in our samples and that the concentration of these vacancies increases with the growth temperature.

D. Magnetization measurements

Magnetic properties of LBMO thin films were measured with the field applied in plane along the [010] direction of the substrate. In Fig. 4, we plot magnetization $M(H)$ hysteresis cycles recorded at 10 K for 30 nm thick films, deposited at 1.10^{-1} mbar and different temperatures. A clear ferromagnetic signal is obtained with a maximum magnetization of 312 emu cm^{-3} at 30 kOe for the film grown at 600°C . This sample displays the highest magnetization despite some traces of a nonmagnetic Bi_2O_3 phase on the XRD scans. Significantly, the magnetization of the films is reduced when T_S increases. The maximal value of the magnetization obtained at 600°C represents roughly half the value for BMO bulk⁸ (542 emu cm^{-3}). We note that our films display reduced magnetizations with respect to those recently reported in 100 nm BMO thin films by Eerenstein *et al.*²⁷ ($2.2 \mu_B/\text{Mn}$, i.e., 330 emu cm^{-3}) or in 70 nm BMO films by Yang *et al.*¹³ ($2.47 \mu_B/\text{Mn}$, i.e., 370 emu cm^{-3}). Nevertheless, these properties are comparable to those reported for BMO thin films of equivalent thicknesses (30 nm) by Ohshima *et al.*¹⁸ We would like to stress that, although spurious Mn-rich phases were detected by AES mappings, these clusters [that may be composed of ferrimagnetic Mn_3O_4 , ($M_S=220 \text{ emu cm}^{-3}$, $T_N=42$ K, Ref. 32)] represent only up to $\sim 12\%$ of the volume of the film and cannot account for the drastic reduction of the magnetic moment with respect to

BMO bulk. Thus, other mechanisms are responsible for the low magnetization of the samples.

It is noteworthy that $M(H)$ cycles display nonzero susceptibility at high fields and the films are difficult to saturate. As identical positive slopes are measured along the $[100]_r$, $[001]_r$, and $[010]_r$ directions (not shown) of the LBMO structure, this behavior is not due to anisotropy effects. This signals the presence of magnetic disorder due, for instance, to a competition between F and AF interactions.

IV. DISCUSSION

From the above analysis, several elements point towards a Bi deficiency in our samples. First, the presence of Mn_3O_4 spurious phases in the films grown at high deposition temperatures ($T_S > 650^\circ\text{C}$ for $P=1.10^{-1}$ mbar), and/or low deposition pressures ($P=1.10^{-2}$ mbar with $T_S=625^\circ\text{C}$), is consistent with a high concentration of cationic A-site vacancies of the AMnO_3 perovskite structure. This feature can thus be either due to a large desorption of nonoxidized Bi during the growth (Bi has a high vapor pressure of $\sim 10^{-3}$ mbar at 580°C) or the decomposition of the Bi_2O_3 phase into O_2 and Bi, due to an instability of this compound at high temperatures.³³ Second, the volume of the LBMO unit cell is fairly reduced with respect to that of bulk BMO [60.61 \AA (Ref. 3)] and decreases when the substrate temperature increases. This behavior can only be due to the formation of cationic vacancies, as oxygen vacancies are known to increase the cell volume of the perovskite structure.²⁸⁻³⁰ Unfortunately, from the experimental point of view, it is difficult to determine the exact content of Bi species in the perovskite phase because the former tends to segregate at the surface of the samples.^{23,24} It is nonetheless possible to estimate the Bi deficiency δ by indirect means, such as the measure of the cell volume. We can, for instance, assume that the cell volume of $\text{Bi}_{1-\delta}\square_{\delta}\text{MnO}_3$ varies in the same fashion as the volume of the $\text{La}_{1-\delta}\square_{\delta}\text{MnO}_3$ system for which experimental data are available.³¹ This is reasonable because La and Bi have similar ionic radii ($r_{\text{La}} \approx 1.22 \text{ \AA}$ and $r_{\text{Bi}} \approx 1.24 \text{ \AA}$).¹⁰ By normalizing to the measured bulk value of BMO, we obtain a linear variation of the BMO unit-cell volume as a function of δ [see inset of Fig. 5(a)].

As it is the specific electronic structure of Bi that is responsible for ferromagnetism in bulk BMO, it is natural to expect a Bi deficiency to be detrimental to ferromagnetism. To get some insight into the relation between magnetization and Bi deficiency, we plot M as a function of the unit-cell volume for several LBMO films, see Fig. 5(a) (black squares). Additionally, the values for two BMO films grown in similar conditions³⁴ (open circles) and bulk BMO have been represented for comparison. There is a clear systematic dependence of the magnetic moment of the films on the cell volume, which is a mark of the strong dependence of the magnetic ordering on the Bi stoichiometry.

To get more quantitative information, we can calculate the magnetic moment of Bi-deficient films within a simple model, taking into account the introduction of $\text{Mn}^{3+}/\text{Mn}^{4+}$ mixed valence for charge conservation purposes and the coupling of neighboring Mn^{3+} and Mn^{4+} sites. The electrical

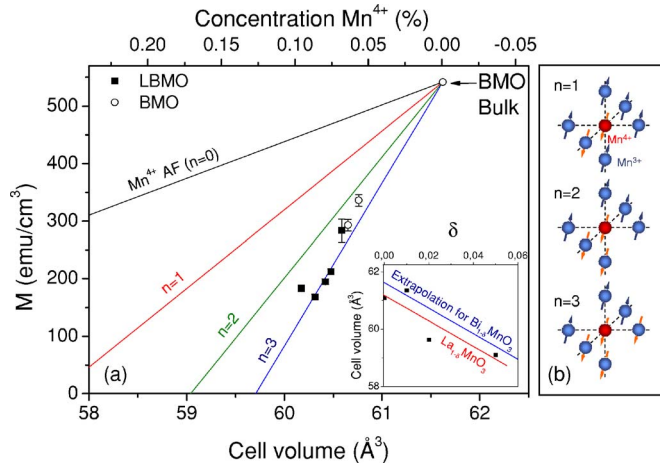


FIG. 5. (Color online) (a) Dependence of the magnetic moment of LBMO and BMO thin films on the cell volume. The lines represent the estimated magnetic moment calculated for a ferromagnetic ordering considering Mn^{4+} ions and Mn^{3+} ions around each Mn^{4+} coupled antiferromagnetically to the macroscopic moment. The inset represents the variation of the unit-cell volume in $\text{La}_{1-\delta}\text{MnO}_3$ and $\text{Bi}_{1-\delta}\text{MnO}_3$ as a function of δ (see text for details). (b) Schematics of the magnetic ordering of the Mn^{3+} around each Mn^{4+} ion in the lattice.

charge conservation imposes the LBMO formula to be written as follows: $\text{La}_{0.1}\text{Bi}_{0.9-\delta}\text{Mn}_{1-3\delta}^{3+}\text{Mn}_{3\delta}^{4+}\text{O}_3$. Hence, each vacancy introduces three tetravalent Mn neighboring sites. These octahedral Mn^{4+} sites are not subjected to a Jahn-Teller distortion and thus contribute to a local destruction of the orbital ordering with the ferromagnetic order locally destroyed as well.

Prior to the calculation of the magnetic moment $M(\delta)$ of LBMO, it is first necessary to examine the coupling between the Mn^{4+} sites and the first Mn^{3+} neighbors. Mn^{4+} has a $t_{2g}^3e_g^0$ configuration and Goodenough-Kanamori-Anderson rules^{35,36} state that a ferromagnetic superexchange occurs when an empty e_g orbital points toward a half filled e_g orbital, such as d_{z^2} on the Mn^{3+} site. On the other hand, the same rules predict an antiferromagnetic coupling when an e_g orbital of the Mn^{4+} points toward an empty $d_{x^2-y^2}$ orbital on a Mn^{3+} site in the direct vicinity. The exchange interaction between Mn^{3+} and Mn^{4+} can thus be either AF or F depending on the local orbital configuration. Assuming a preservation of the local orbital order of BMO, each Mn^{4+} site would be coupled AF to the surrounding Mn^{3+} matrix because of the occurrence of four antiferromagnetic vs two ferromagnetic superexchange interactions with the first neighbors. The situation is more complex when the orbital orientation of the first Mn^{3+} neighbors surrounding each Mn^{4+} site is random: competing F/AF interactions and thus a strong spin frustration should be expected. In an idealized case, we can consider that in each octahedron composed of a central Mn^{4+} with Mn^{3+} ions on the vertices, some of the Mn^{3+} are still coupled ferromagnetically to the rest of the crystalline network of BMO. On the other hand, the Mn^{4+} as well as several neighboring Mn^{3+} shall be considered as coupled antiferromagnetically to the surrounding Mn^{3+} matrix.

From the concentration of Bi vacancies δ estimated from the unit-cell volume, it is straightforward to calculate the

concentration of Mn^{4+} corresponding to the cell volume of our LBMO and BMO films (see the top axis of Fig. 5). By considering the case of an unperturbed orbital order with Mn^{4+} ions coupled antiferromagnetically to the Mn^{3+} matrix, one obtains the relationship $M(\delta)$ (in μ_B/Mn): $M=4-21\delta$, from which we calculate the black curve ($n=0$) on Fig. 5. It is noticeable that the calculated moment is still too high as compared to the experimental values. This disagreement is certainly due to the frustration of the Mn^{3+} matrix in the vicinity of a Bi vacancy. We thus consider the formerly exposed case of an AF orientation of the Mn^{4+} site as well as several Mn^{3+} neighbors coupled AF with the macroscopic moment of the film, shown in the schematics of Fig. 5(b). The magnetic moment takes the following form: $M=4[1-3(1+2n)\delta]-9\delta$, where n is the average number of sites surrounding the Mn^{4+} sites that are coupled AF to the BMO matrix. As shown in Fig. 5(a), the calculated moment for $n=1$ and $n=2$ is still overestimating the experimental data, while for $n=3$ the theoretical curve is in rather good agreement with the magnetic moment of our BMO and LBMO films. If we allow n to take noninteger values, the best fit is obtained for an average number of $n \approx 2.8$ AF-coupled Mn^{3+} neighbors.

This very simple model is thus able to provide a semi-quantitative description of the magnetization of the films by taking into account the local destruction of the orbital ordering of the Mn^{3+} d_{z^2} orbitals around Mn^{4+} sites, the latter resulting from the presence of Bi vacancies. The resulting destruction of ferromagnetism appears to be more drastic in LBMO and BMO thin films than for the $\text{Bi}_x\text{Sr}_{1-x}\text{MnO}_3$ system³⁷ at low Mn^{4+} content ($<10\%$). This is likely to be due to the fact that Bi vacancies produce a long-range destruction of the orbital ordering, while the perturbation resulting from Sr substitution of Bi sites is more localized. It is also worthwhile mentioning that the estimated amount of Bi vacancies tops 3%–4% in the most Bi-deficient LBMO films which is hardly detectable with usual chemical characterization techniques such as energy dispersive x-ray spectroscopy, Auger, or x-ray photoelectron spectroscopy.

The presence of two different valences on the Mn site is clear from the XAS results shown in Fig. 6. Such measurements, shown on Fig. 6, have been performed at 4 K on a 30 nm LBMO thin film grown at 625 °C and 1.10^{-1} mbar. The XAS spectra at the L_3 edge show three peaks, which reflects the concomitant presence of Mn^{3+} and Mn^{4+} .³⁸ In the XMCD spectra, a negative contribution from 642 to 646 eV is recognizable and can be ascribed to the ferromagnetic ordering of the Mn^{3+} sites. An interesting feature is the positive contribution at 644 eV to the XMCD curve, which can be interpreted as due to the presence of Mn sites with a valence different from 3+, whose resulting moment points in the direction opposite to the magnetization of the Mn^{3+} matrix. The features of the XMCD spectra reported here resemble those reported and calculated for a Mn-based molecular superparamagnet ($\text{Mn}_{12}\text{-ac}$) in which the moments of Mn^{3+} and Mn^{4+} sites are antiparallel.³⁸ It is, thus, reasonable to assert that the XMCD signal of LBMO films result from a matrix of ferromagnetically coupled Mn^{3+} sites with inclusions of Mn^{4+} sites coupled AF to the latter matrix, which is

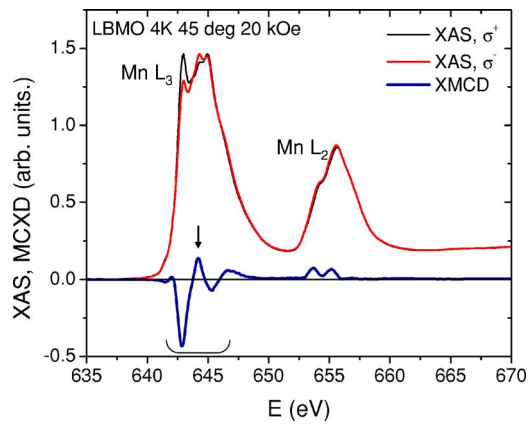


FIG. 6. (Color online) XAS spectra for left and right circular polarization (σ^+ and σ^-) and x-ray magnetic dichroic signal recorded at 10 K, in a field of 20 kOe with a beam incidence of 45° in TEY mode.

a strong argument in favor of our model. Finally, we note that, as in the $\text{Bi}_x\text{Sr}_{1-x}\text{MnO}_3$ system, the presence of a mixed Mn valence in Bi-deficient LBMO does *not* result in a transition to a conductive state³⁹ (as opposed to the case of $\text{La}_x\text{Sr}_{1-x}\text{MnO}_3$), which is likely to be related to the distortion caused by the Bi $6s$ lone pairs.⁸

V. SUMMARY AND CONCLUSIONS

The structure and magnetic properties of $\text{La}_{1-x}\text{Bi}_x\text{MnO}_3$ ($x \leq 0.1$) thin films have been investigated. It is shown that

the volume of the films is strongly reduced with respect to bulk BiMnO_3 which is ascribed to the presence of a few percent of Bi vacancies. Furthermore, a clear correlation between the structural properties and the saturation moment of the films is evidenced. A simple model based on Goodenough-Kanamori-Anderson rules is then developed to explain the reduced magnetization of the films. A good agreement between experimental data and this model is obtained by taking into account the presence of Mn^{4+} sites consecutive to Bi deficiency as well as the magnetic disorder due to the local destruction of the orbital ordering around the latter sites. Finally, further evidence of an antiferromagnetic ordering of Mn^{4+} in the Mn^{3+} matrix of $\text{La}_{0.1}\text{Bi}_{0.9}\text{MnO}_3$ is provided by x-ray magnetic circular dichroism measurements. This study emphasizes the strong dependence of the ferromagnetic ordering of $\text{La}_{0.1}\text{Bi}_{0.9}\text{MnO}_3$ on the Bi stoichiometry and may provide pathways for the further improvement of the magnetic properties of BiMnO_3 thin films.

ACKNOWLEDGMENTS

The authors would like to thank P. Ohresser and V. Cros for their assistance with XAS and XMCD measurements and interpretation. This study was partially supported by the Picasso France-Spain program (EGIDE), the Spanish projects NAN2004-9094 and MAT2005-05656, the project FEMMES of the French Agence Nationale de la Recherche (ANR-05-1-45147), the EU STREP MaCoMuFi (Contract No. FP6-NMP3-CT-2006-033221), and the European Science Foundation THIOX program.

*Electronic address: mgajek@berkeley.edu

¹W. Eerenstein, N. D. Mathur, and J. F. Scott, *Nature (London)* **442**, 759 (2006).
²M. Gajek, M. Bibes, S. Fusil, K. Bouzehouane, J. Fontcuberta, A. Barthélémy, and A. Fert, *Nat. Mater.* **6**, 296 (2007).
³V. A. Bokov, I. E. Myl'nikova, S. A. Kizhaev, M. F. Bryzhina, and N. A. Grigoryan, *Sov. Phys. Solid State* **7**, 2993 (1966).
⁴F. Sugawara, S. Iida, Y. Syono, and A. Akimoto, *J. Phys. Soc. Jpn.* **25**, 1553 (1968).
⁵A. Moreira dos Santos, S. Parashar, A. R. Raju, Y. S. Zhao, A. K. Cheetham, and C. N. R. Rao, *Solid State Commun.* **122**, 49 (2002).
⁶J. Y. Son, B. G. Kim, C. H. Kim, and J. H. Cho, *Appl. Phys. Lett.* **84**, 4971 (2004).
⁷A. Sharan, J. Lettieri, Y. Jia, W. Tian, X. Pan, D. G. Schlom, and V. Gopalan, *Phys. Rev. B* **69**, 214109 (2004).
⁸H. Chiba, T. Atou, and Y. Syono, *J. Solid State Chem.* **132**, 139 (1997).
⁹E. O. Wollan and W. C. Koehler, *Phys. Rev.* **100**, 545 (1955).
¹⁰R. D. Shannon and C. T. Prewitt, *Acta Crystallogr., Sect. B: Struct. Crystallogr. Cryst. Chem.* **25**, 925 (1969).
¹¹R. Seshadri and N. A. Hill, *Chem. Mater.* **13**, 2892 (2001).
¹²A. F. Moreira dos Santos, A. K. Cheetham, T. Atou, Y. Syono, Y. Yamaguchi, K. Ohoyama, H. Chiba, and C. N. R. Rao, *Phys. Rev. B* **66**, 064425 (2002).

¹³C.-H. Yang, J. Koo, C. Song, T. Y. Koo, K.-B. Lee, and Y. H. Jeong, *Phys. Rev. B* **73**, 224112 (2006).
¹⁴O. Yu. Gorbenko, S. V. Samoilenov, I. E. Graboy, and A. R. Kaul, *Chem. Mater.* **14**, 4026 (2002).
¹⁵I. O. Troyanchuk, O. S. Mantyt'skaja, H. Szymczak, and M. Yu. Shvedun, *Low Temp. Phys.* **28**, 569 (2002).
¹⁶T. Ogawa, H. Shindo, H. Takeuchi, and Y. Koizumi, *Jpn. J. Appl. Phys., Part 1* **45**, 8666 (2006).
¹⁷W. Eerenstein, F. D. Morrison, J. Dho, M. G. Blamire, and J. F. Scott, *Science* **307**, 1203a (2005).
¹⁸E. Ohshima, Y. Saya, M. Nantoh, and M. Kawai, *Solid State Commun.* **116**, 73 (2000).
¹⁹A. F. Moreira dos Santos, A. K. Cheetham, W. Tian, X. Pan, Y. Jia, N. J. Murphy, J. Lettieri, and D. G. Schlom, *Appl. Phys. Lett.* **84**, 91 (2004).
²⁰C.-H. Yang, T. Y. Koo, S.-H. Lee, C. Song, K.-B. Lee, and Y. H. Jeong, *Europhys. Lett.* **74**, 348 (2006).
²¹S. Fujino, M. Murakami, S.-H. Lin, L. G. Salamanca-Riba, M. Wuttig, and I. Takeuchi, *J. Appl. Phys.* **101**, 013903 (2007).
²²M. Gajek, M. Bibes, A. Barthélémy, K. Bouzehouane, S. Fusil, M. Varela, J. Fontcuberta, and A. Fert, *Phys. Rev. B* **72**, 020406(R) (2005).
²³M. Alexe, J. F. Scott, C. Curran, N. D. Zakharov, D. Hesse, and A. Pignolet, *Appl. Phys. Lett.* **73**, 1592 (1998).
²⁴H. Béa, M. Bibes, A. Barthélémy, K. Bouzehouane, E. Jacquet,

- A. Khodan, J.-P. Contour, S. Fusil, F. Wyczisk, A. Forget, D. Lebeugle, D. Colson, and M. Viret, *Appl. Phys. Lett.* **87**, 072508 (2005).
- ²⁵H. Béa, M. Bibes, S. Fusil, K. Bouzehouane, E. Jacquet, K. Rode, P. Bencok, and A. Barthélémy, *Phys. Rev. B* **74**, 020101(R) (2006).
- ²⁶P. A. Joy, C. R. Shankar, and S. K. Date, *J. Phys.: Condens. Matter* **14**, L663 (2002).
- ²⁷W. Eerenstein, F. D. Morrison, J. F. Scott, and N. D. Mathur, *Appl. Phys. Lett.* **87**, 101906 (2005).
- ²⁸H. Okamoto, H. Fjellvåg, H. Yamauchi, and M. Karppinen, *Solid State Commun.* **137**, 522 (2006).
- ²⁹T. Zhao, F. Chen, H. Lu, G. Yang, and Z. Chen, *J. Appl. Phys.* **87**, 7442 (2000).
- ³⁰C. H. Park and D. J. Chadi, *Phys. Rev. B* **57**, R13961 (1998).
- ³¹J. M. D. Coey, M. Viret, and S. von Molnár, *Adv. Phys.* **48**, 167 (1999).
- ³²K. Dwight and N. Menyuk, *Phys. Rev.* **119**, 1470 (1960).
- ³³J. Picon, *J. Pharm. Chim.* **10**, 481 (1929).
- ³⁴M. Gajek, Ph.D. thesis, Université Paris VI, 2006.
- ³⁵P. W. Anderson, *Phys. Rev.* **79**, 350 (1950).
- ³⁶J. Goodenough, *Phys. Rev.* **100**, 564 (1955).
- ³⁷T. Atou, H. Chiba, K. Ohoyama, Y. Yamaguchi, and Y. Syono, *J. Solid State Chem.* **145**, 639 (1999).
- ³⁸R. Moroni, Ch. Cartier dit Moulin, G. Champion, M.-A. Arrio, Ph. Sainctavit, M. Verdaguer, and D. Gatteschi, *Phys. Rev. B* **68**, 064407 (2003).
- ³⁹M. Gajek, M. Bibes, M. Varela, J. Fontcuberta, G. Herranz, S. Fusil, K. Bouzehouane, A. Barthélémy, and A. Fert, *J. Appl. Phys.* **99**, 08E504 (2006).